IEEE Photonics Journal
An IEEE Photonics Society Publication

Open Access

Roughness Estimation of Multimode Rectangular Optical Waveguide Based on the Scattering Loss Difference Between SMFW and MMFW Structures

Volume 9, Number 2, April 2017

Chuanlu Deng
Tingyun Wang
Jiamin Chen
Chengbo Mou
Xiaobei Zhang, ***Member, IEEE***
Xinjie Yan
Fufei Pang

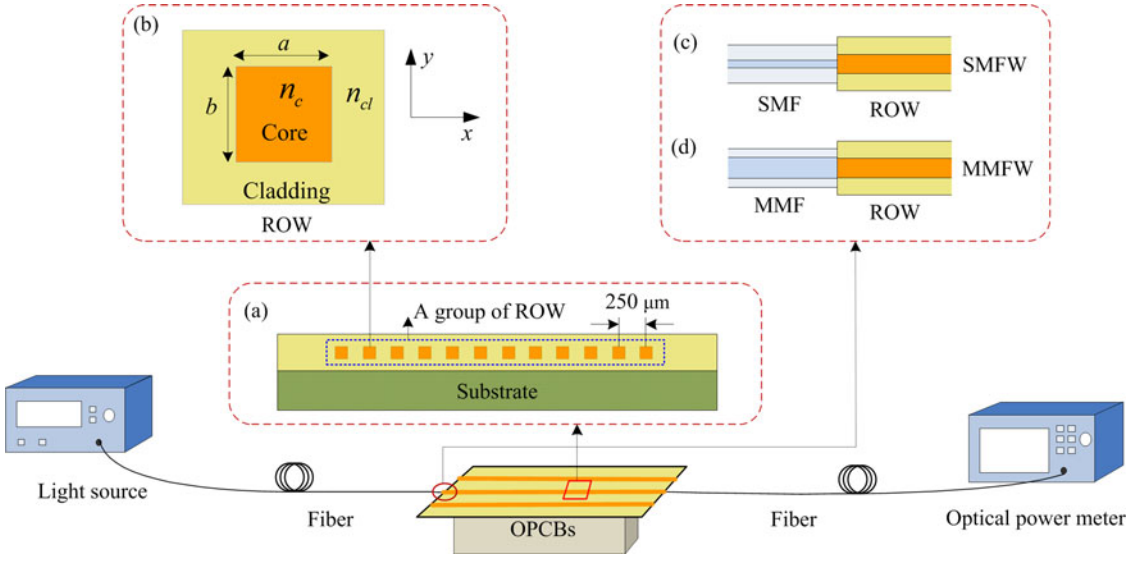

DOI: 10.1109/JPHOT.2017.2682120
1943-0655

Roughness Estimation of Multimode Rectangular Optical Waveguide Based on the Scattering Loss Difference Between SMFW and MMFW Structures

Chuanlu Deng, Tingyun Wang, Jiamin Chen, Chengbo Mou, Xiaobei Zhang, *Member, IEEE*, Xinjie Yan, and Fufei Pang

Key Laboratory of Specialty Fiber Optics and Optical Access Networks, School of Communication and Information Engineering, Shanghai University, Shanghai 200072, China

DOI:10.1109/JPHOT.2017.2682120

Manuscript received January 25, 2017; revised March 8, 2017; accepted March 9, 2017. Date of publication March 15, 2017; date of current version March 27, 2017. This work was supported in part by the Science and Technology Commission of Shanghai Municipality (16511104300) and in part by the Education Commission Innovation of Shanghai Municipality (14ZZ093). Corresponding author: T. Wang (e-mail: tywang@shu.edu.cn).

Abstract: Based on the scattering loss difference between the single-mode-fiber-optical-waveguide (SMFW) and multimode-fiber-optical-waveguide (MMFW) structures, a method to estimate the roughness of multimode rectangular optical waveguide (ROW) is proposed. Based on the analysis of the mode coupling characteristics of the SMFW structure and the MMFW structure, the coupling efficiency of higher order mode of the ROW for the MMFW structure is larger than that of the SMFW structure. However, it is reversed for the lower order mode. By further analyzing the mode scattering loss coefficients of ROW induced by roughness, it is found that the total scattering loss for the SMFW structure is less than that for the MMFW structure, which can be used to estimate the roughness. The experimental results show that the roughness is 248.67 nm when the waveguide length is 75 mm and the scattering loss difference is 0.31dB. As the roughness is 275.37 nm by the 3-D optical profiler, this implies that the method is effective. Compared to the conventional methods, the method has many advantages, such as convenience, high efficiency, and ability for large measurement area.

Index Terms: Roughness, polymer waveguides, optical interconnects.

1. Introduction

With the rapid development of high performance computing (HPC) [1], big data center [2], and broadband communication [3], the electrical interconnect technologies are rapidly approaching their fundamental bandwidth limitation of ∼50 Gb/s [4]. The waveguide technologies for optical printed circuit boards (OPCBs) interconnects have been recently attracted wide attentions [5], [6]–[10] attributing to their unique advantages of high transmission rate, electromagnetic interference immunity, high density integration capability, low power consumption, and so on. At present, the transmission loss of optical waveguide can be as low as 0.04 dB/cm at 850 nm [9]. The coupling devices based on different structures such as micro-mirror [5], optical element [8], and flexible waveguide [5] applied to OPCBs have been fabricated. The demonstration based on OPCBs technologies shows the good performance with a bit error rate of less than 10^{-12} at data

rates of 40 Gb/s over waveguide lengths of 100 mm [10]. Moreover, optical waveguide also have been widely designed as the key optical components such as coupler [11], modulator [12], amplifier [13], sensor [14], and (de)multiplexer [15]. All these optical waveguide components are essential to the development of optical waveguide integration on printed circuit boards (PCBs) in future. OPCBs technologies are promising to become one of the main interconnection technologies in the future.

At present, the good performance of waveguide materials can meet the requirement of waveguide applications [16]. Nevertheless, the larger transmission loss due to the outdated preparation technology of waveguide still limits the applications of waveguide. The roughness of waveguide core is the main issue [17]–[22]. It leads to not only the coupling between the guided modes [18] but also the coupling between the guided modes and the radiation modes [17], [19]–[22], resulting in the scattering loss. For the rectangular optical waveguide (ROW), the scattering loss is up to 0.06 dB/cm when the sidewall roughness is 50 nm [17]. Moreover, the roughness also degrades the characteristics of optical waveguide components such as decreasing the coupling efficiency of waveguide coupler [11], degrading the characteristics of waveguide microring resonator [14], and reducing the internal gain of waveguide amplifier [13]. Therefore, it is essential to determine the accurate roughness value, which can guide the optimization of waveguide design. Roughness generally is evaluated accurately by using tools such as the atomic force microscopy (AFM) [17], [22] and 3D optical profiler [23]. However, the measurement length is limited to be on the order of tens of or few microns [17], [22], and the measurement is insufficient to reveal the general situation. If the general evaluation is carried out across the whole surface of waveguide core, it will be time-consuming. Due to the special position of waveguide sidewall, many measurement difficulties will also greatly increase. Furthermore, the waveguide core polluted by the dust in air will induce the large scattering loss because the evaluation begins after the fabrication of waveguide core. Hence, it is desirable to find an effective method to examine the roughness of waveguide core.

In this paper, we have proposed and demonstrated a method to estimate the roughness of ROW, based on the differential scattering loss induced by the roughness between the SMF-optical-waveguide (SMFW) configuration and the MMF-optical-waveguide (MMFW) configuration. First, the mode coupling characteristics for the SMFW and for the MMFW structures are discussed in detail. Then the influence on mode scattering loss coefficients of ROW induced by roughness has been analyzed. After that, a method to estimate the roughness of the ROW is studied. Finally, the experimental results agree well with the theoretical data, which implies the method is effective. Our work can provide the theoretical support for the roughness estimation of the ROW.

2. Principle

The schematic structure of OPCBs interconnection is shown in Fig. 1. Many groups of optical waveguides are fabricated on the normal PCBs. There are 12 channel waveguides in each group, and the core distance is 250 μm, which is shown in Fig. 1(a). Multi-mode ROW is a common waveguide structure, while the diagram of the cross-section is shown in Fig. 1(b). The core has a rectangular shape with the width a of 50 μm and the height b of 50 μm. The refractive indices of core n_c and cladding n_{cl} is 1.51 and 1.48, respectively. Optical signal propagates from light source to a short piece of standard optical fiber (single-mode fiber, SMF, or multi-mode fiber, MMF) followed by the multimode ROW. The transmitted signal is then monitored by a power meter through another piece of MMF. The optical power carried by each mode in multimode ROW is determined by the mode coupling efficiency. Two kinds of coupling mechanisms between the fiber and ROW namely SMFW and MMFW have been shown in Fig. 1(c) and (d), respectively. The signal wavelength λ is 850 nm.

Two kinds of modes exist such as E^x_{mn} and E^y_{mn} (m and n as the mode orders in x and y directions respectively) in multimode ROW [24]. Because E^x_{mn} and E^y_{mn} modes degenerate at the same mode order, only E^x_{mn} mode will be considered in this paper.

In a real waveguides, there is irregular distribution at the core-cladding interface, which can be characterized by the roughness σ. Fig. 2 shows the diagram of ROW core with the distortion characterized by the roughness function $f(z)$. The field components of E^x_{mn} mode have the relation

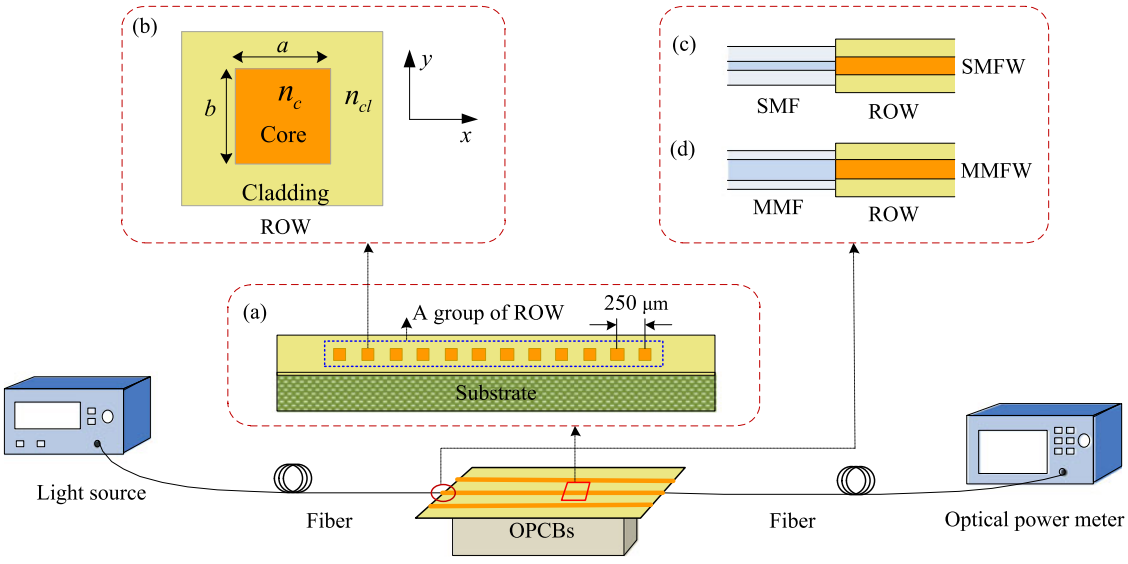

Fig. 1. Diagram of OPCBs interconnection. (a) Diagram of OPCBs with 12 channel waveguides in each group, (b) diagram of the cross-section of the multimode ROW, (c) SMFW structure, and (d) MMFW structure.

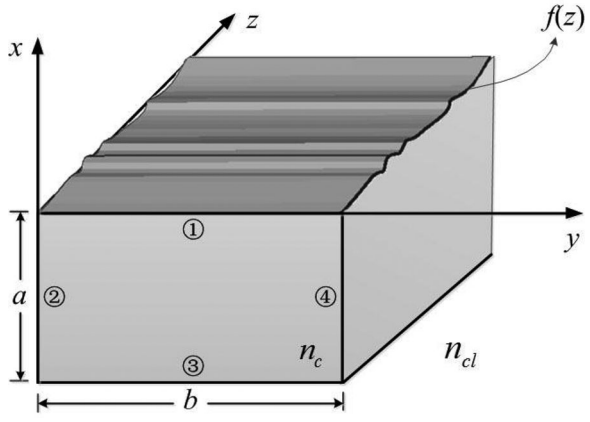

Fig. 2. Diagram of ROW core with distortion function $f(z)$.

as $E_y \ll E_z \ll E_x$ [25]. Therefore, the coupling coefficients between the guided modes and the radiation modes caused by the aforementioned waveguide irregularities can be expressed as [25]

$$K_{mn,\rho} = \frac{\omega\varepsilon_0}{4iP}\int_{-\infty}^{\infty}\int_{-\infty}^{\infty}\left(n^2 - n_0^2\right)\vec{E}^{x*}_{mn}\vec{E}^{x}_{\rho}dxdy \tag{1}$$

where ω is the angular frequency of light, ε_0 is the dielectric constant of vacuum, P is the power factor, $\vec{E}^{x}_{mn}$ is the electric field of E^{x}_{mn} mode along the x direction, and $\vec{E}^{x}_{\rho}$ is the electric field of the radiation modes along the x direction [25].

The scattering loss coefficient α_{mn} of E^{x}_{mn} mode induced by σ is a characteristic parameter to describe the influence on the transmission loss of ROW. According to standard perturbation theory,

TABLE 1
Parameters of SMF and MMF

Fiber	The refractive index of core	The refractive index of cladding	Core radius
SMF	1.4681	1.4628	4.5 μm
MMF	1.4662	1.45	25 μm

α_{mn} can be expressed as [25]

$$\alpha_{mn} = \iint \sum_{i=1}^{4} \left|K^{i}_{mn,\rho}(\kappa, \upsilon)\right|^2 \left\langle \left|F^{i}\left(\beta_{mn} - \beta_{\rho}\right)\right|^2 \right\rangle d\kappa d\upsilon \tag{2}$$

where $K^{i}_{mn,\rho}(\kappa, \upsilon)$ and $\langle|F(\beta_{mn} - \beta_{\rho})|^2\rangle$ are the expression with relation to the roughness σ and the correlation length L_c, which is discussed in Appendix A.

To take the mode scattering loss into account, the transmitting mode field distribution in ROW can be expressed as $\psi_{mn}(x, y)\exp(-\alpha_{mn}L)$. Then, the scattering loss at ROW output [25] for the SMFW structure can be written as

$$Loss^{(s)} = -10\log_{10}\left\{\sum_{m=1}^{M}\sum_{n=1}^{N}\left|\eta_{s\to mn}\exp\left(-\alpha_{mn}L\right)\right| / \sum_{m=1}^{M}\sum_{n=1}^{N}\left|\eta_{s\to mn}\right|\right\} \tag{3}$$

where $\eta_{s_{mn}}$ is the coupling efficiency between LP_{01} mode of SMF and E^{x}_{mn} mode of ROW, with L as the waveguide length.

For the MMFW structure, the scattering loss at ROW output can be written as

$$Loss^{(m)} = -10\log_{10}\left\{\sum_{q=1}^{Q}\eta_{l\to q}\left[\sum_{m=1}^{M}\sum_{n=1}^{N}\left|\eta_{q\to mn}\exp\left(-\alpha_{mn}L\right)\right|\right] / \sum_{q=1}^{Q}\eta_{l\to q}\left|\sum_{m=1}^{M}\sum_{n=1}^{N}\left|\eta_{q\to mn}\right|\right|\right\} \tag{4}$$

where $\eta_{q\to mn}$ is the coupling efficiency between LP_{0q} mode of MMF and E^{x}_{mn} mode of ROW, and $\eta_{l\to q}$ is the coupling efficiency between light source and LP_{0q} mode of MMF. The mathematical derivations of coupling efficiencies are summarized in Appendix B.

Therefore, the total scattering loss coefficient α_{total} [25] can be expressed as

$$\alpha^{(x)}_{total} = Loss^{(x)}/L\,,\ (x = s, m)\,. \tag{5}$$

Roughness can also lead to the mode coupling between the guided modes of ROW. However, the maximum coupling coefficient only reaches to 10^{-6} when $\sigma = 70$ nm [18]. Due to the linear dependency on σ^2 [18], the maximum coupling coefficient with $\sigma = 200$ nm is estimated to be 10^{-5}. Thus it is negligible in our following analysis.

3. Simulation

Table 1 shows the typical parameters of SMF and MMF used in our simulation.

3.1 Coupling Characteristics

When SMF is coupled to the ROW, a certain proportion of optical power is transferred to E^{x}_{mn} mode. The coupling efficiency between LP_{01} mode of SMF and E^{x}_{mn} mode of ROW with even mode order is quite small due to the different odd-even characteristics of their filed distributions [24].

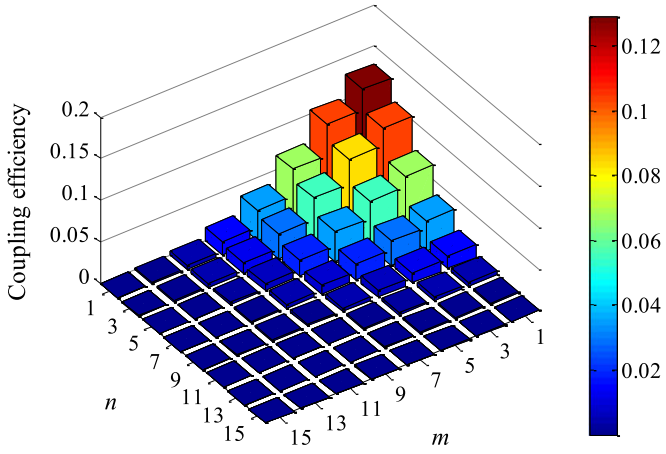

Fig. 3. Mode coupling efficiencies between SMF and ROW.

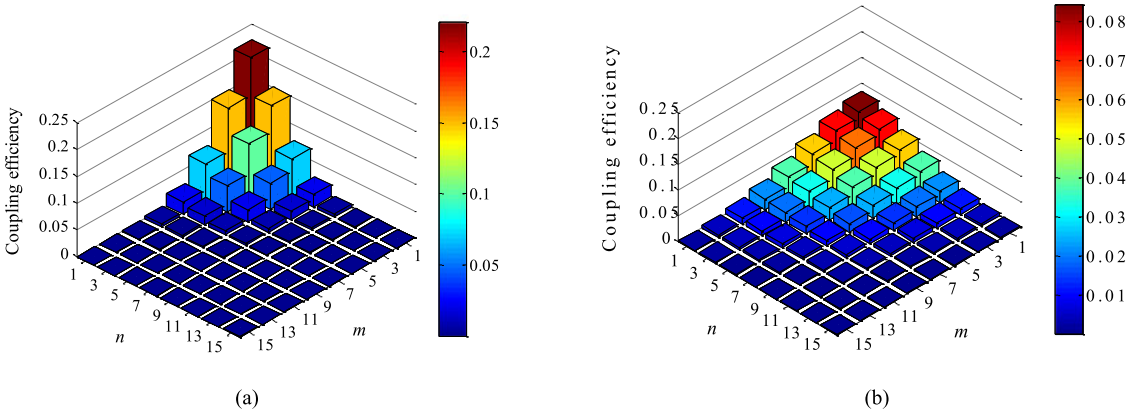

Fig. 4. Mode coupling efficiencies between MMF and ROW. (a) Mode field radius $\omega_l = 5\,\mu$m, and (b) mode field radius $\omega_l = 3\,\mu$m.

The field power from SMF is mostly transferred to the odd order modes of ROW. The following numerical calculation only considers E^x_{mn} mode of ROW with an odd mode order. Fig. 3 shows the characteristics of E^x_{mn} mode coupling efficiencies. It is clear that the coupling efficiency decreases as increasing mode orders (m, n). In general, the coupling efficiency depends on the similarity between two mode field distributions. For example, when the mode order is $m = n = 1$, the E^x_{11} mode coupling efficiency is 12.99%. And when the mode order is $m = n = 9$, the E^x_{99} mode coupling efficiency is 0.18%. Thus, the coupling efficiency of higher-order mode can be neglected.

When MMF is coupled to ROW, the mode coupling efficiency of ROW is related to all modes of MMF. However, the mode power distribution of MMF is also related to light source. The mode coupling efficiencies between MMF and ROW with the mode field radius of VCSEL as $\omega_l = 5\,\mu$m and $\omega_l = 3\,\mu$m is shown in Fig. 4(a) and (b), respectively. On the whole, the coupling characteristic of MMFW structure is similar to that of SMFW structure. The coupling efficiency of lower-order mode with $\omega_l = 5\,\mu$m is higher than that with $\omega_l = 3\,\mu$m, while the coupling efficiency of higher-order modes is the other way around. Therefore, the mode coupling characteristics of ROW can be determined by the incident light beam properties. The larger the mode field radius of VCSEL is, the larger the coupling efficiency of lower-order mode is. This is because the correlation of two mode field distributions is greater, especially for the fundamental mode of waveguide.

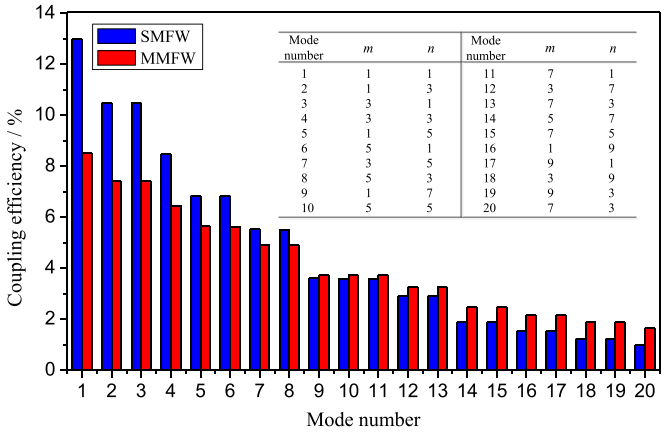

Mode number	m	n	Mode number	m	n
1	1	1	11	7	1
2	1	3	12	3	7
3	3	1	13	7	3
4	3	3	14	5	7
5	1	5	15	7	5
6	5	1	16	1	9
7	3	5	17	9	1
8	5	3	18	3	9
9	1	7	19	9	3
10	5	5	20	7	3

Fig. 5. Comparison of mode coupling efficiencies between SMFW and MMFW structures with $\omega_l = 3\,\mu$m.

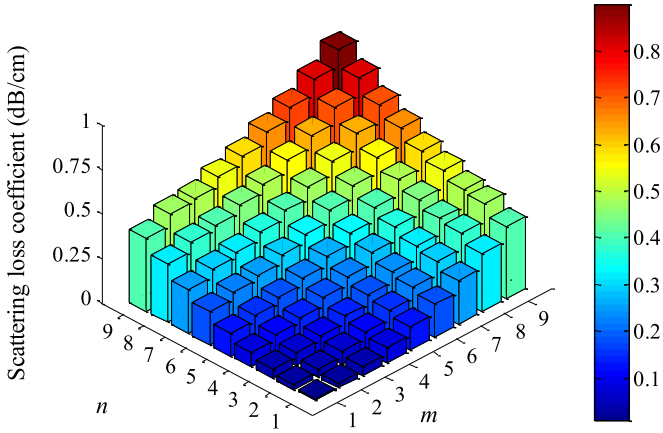

Fig. 6. Mode scattering loss coefficients for different mode order with $\sigma = 100$ nm and $L_c = 2\,\mu$m.

The simulation data from Figs. 3 and 4(b) is aggregated in Fig. 5, where the abscissa indicates the mode order of ROW, and the histogram color for the SMFW and MMFW structures are red and blue respectively. The mode coupling efficiency vary small with increasing mode order. Moreover, the coupling efficiency of E^x_{mn} mode with mode number of less than 9 ($m = 1$, $n = 7$) for the SMFW structure is larger than that of E^x_{mn} modes for the MMFW structure, but it is reversed for E^x_{mn} modes with mode number of more than 9. The mode coupling efficiency characteristics for the SMFW and MMFW structures implies the differential scattering loss induced by roughness σ.

3.2 Mode Scattering Loss

All guided modes of the ROW are influenced by the roughness σ. Different modes have different scattering loss coefficients. The correlation length L_c can be directly calculated from the experimental measurements [17], [22]. For the multimode polymer ROW, it has been proved theoretically and experimentally that L_c of 2 μm is more accurate in the calculation of scattering loss coefficient [26]. In our simulation, the core surface roughness is assumed to be the same as the core sidewall roughness. When σ is 100 nm, the distribution of mode scattering loss coefficients of the ROW is shown in Fig. 6. The mode scattering loss coefficient increases with increasing mode order. The mode scattering loss coefficient is symmetric on the mode order ($m = n$) fundamentally. For

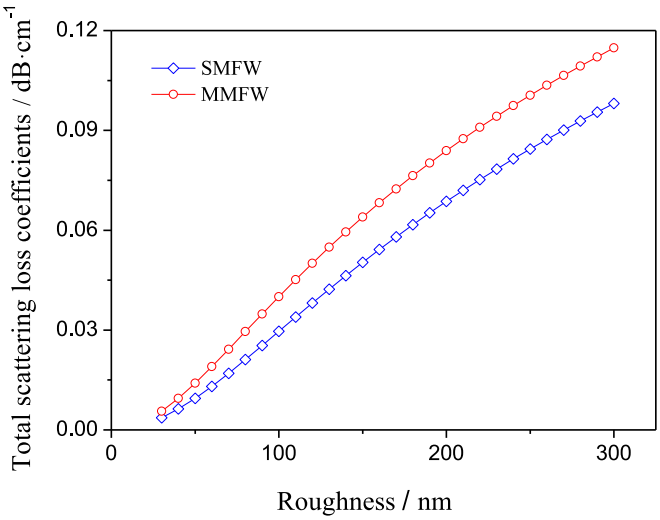

Fig. 7. Total scattering loss coefficient of ROW as different roughness with $L_c = 2\,\mu$m.

example, the scattering loss coefficient of E^x_{13} mode and E^x_{31} mode is 2.527×10^{-2} dB/cm and 2.531×10^{-2} dB/cm, respectively, which is very close.

When L_c is 2 μm and L is 100 cm, the total scattering loss coefficients α_{total} with σ for the SMFW and MMFW structures are plotted in Fig. 7. It shows that α_{total} increases with σ for the two coupling structures. When σ is approximately lower than 300 nm, α_{total} is on the order of magnitude of 10^{-2} dB/cm. And when σ is higher than 300 nm, it is on the order of magnitude of 10^{-1} dB/cm. It is clear that α_{total} for the MMFW structure is also greater than that for the SMFW structure with the same σ. The larger σ is, the larger the difference of α_{total} is. The difference is very small when σ is 30 nm. Given σ from 30 nm to 300 nm, α_{total} increases from 3.65×10^{-3} dB/cm to 9.8×10^{-2} dB/cm for the SMFW structure and from 5.6×10^{-3} dB/cm to 1.15×10^{-1} dB/cm for the MMFW structure. The difference of scattering loss is approximately 1-1.7 dB when σ is from 100 nm to 300 nm and L is 100 cm. If σ is up to 300 nm, the total scattering loss is 9.81 dB for the SMFW structure and 11.48 dB for the MMFW structure respectively, which means that the roughness is a disadvantage for the transmission characteristic of ROW.

Based on the scattering loss difference between the SMFW and MMFW structures, a better method to estimate the roughness of ROW core can be introduced as the following.

3.3 A Method to Estimate Roughness

From (1) and (2), the scattering loss induced by the roughness σ is related to the mode propagation constant β_{mn} of ROW, the waveguide length L and the mode efficiency η between fiber and ROW. In case that the difference of scattering loss δ and the related parameters are defined, the roughness σ can be calculated by the following equation:

$$\delta = Loss^{(m)}\left(\sum_m^M \sum_n^M \beta_{mn}, L, \sigma\right) - Loss^{(s)}\left(\sum_m^M \sum_n^M \beta_{mn}, L, \sigma\right) \tag{6}$$

where $Loss^{(m)}(\sum_m^M \sum_n^M \beta_{mn}, L, \sigma)$ and $Loss^{(s)}(\sum_m^M \sum_n^M \beta_{mn}, L, \sigma)$ is the scattering loss for the MMFW and SMFW structures, respectively. When parameters (β_{mn}, L, η) are determined, σ can be calculated by the complex numerical calculation for the certain δ. In order to calculate easily, (6) can be

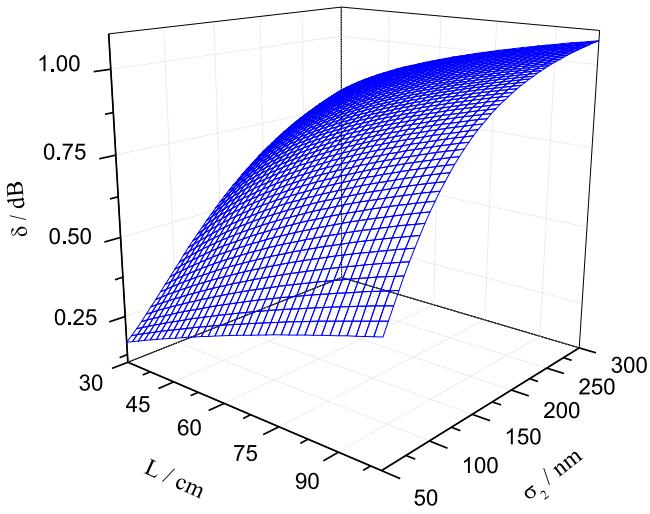

Fig. 8. Difference of scattering loss between for SMFW structure and for MMFW structure with σ_2 (50 nm–300 nm) and L (30 mm–100 mm) when $\omega_l = 3\,\mu$m and $\sigma_1 = 50$ nm.

written as

$$f(\sigma) = \delta - \left[L\,oss^{(m)} \left(\sum_m^M \sum_n^M \beta_{mn}, L\,, \sigma \right) - L\,oss^{(s)} \left(\sum_m^M \sum_n^M \beta_{mn}, L\,, \sigma \right) \right]. \tag{7}$$

When $f(\sigma)$ with the test root σ is zero, the root σ exactly is the solution to this (7).

Generally, the core sidewall roughness σ_2 is much greater than the core surface roughness σ_1 [17] in the real ROW. Fig. 8 further describes the difference of scattering loss between the SMFW and MMFW structures with σ_2 (50 nm–300 nm) and L (30 mm–100 mm), when σ_1 is 50 nm and ω_l is 3 μm. It can be clear that the difference of scattering loss increases with σ_2 and L increasing. Assuming that σ_2 is 200 nm and L is 100 cm, α_{total} for MMFW structure can be calculated as 4.94×10^{-2} dB/cm and 4.60×10^{-2} dB/cm when σ_1 of 50 nm is considered and not considered respectively, which means that the scattering loss difference is very small. When σ_2 is larger, the influence induced by σ_1 can be neglected.

4. Experiment

The sample of ROW uncoated upper cladding with the length of 75 mm is fabricated by the photolithography method. The core material (LightLink™ XP-6701A) and the cladding material (LightLink™ XH-100145) are produced by Dow. The refractive indices of core n_c of 1.51 and cladding n_{cl} of 1.48 are provided. The microscopic appearance of ROW by 3D optical profiler (Sensofar-Tech, SNEOX) is shown in Fig. 9(a). Fig. 9(b) displays the enlarged details of core surface and core sidewall. Fig. 9(c) and (d) depicts the core surface roughness of 52.67 nm and the core sidewall roughness of 252.10 nm, respectively. The core sidewall roughness is larger more than the core surface roughness. Therefore, the scattering loss is induced by the core sidewall roughness mostly. In order to obtain the exact value of core sidewall roughness, the random values in Table 2 along core has been measured accurately. The mean square root of 275.37 nm is calculated. Further, the transmission loss $L\,oss_t^{(s)}$ and $L\,oss_t^{(m)}$ is measured as 3.81 dB and 4.12 dB respectively. As shown in the Section 3.3 above, the roughness σ is calculated as 248.67 nm. The results based on the proposed method well conform to the measured data by 3-D optical profiler.

In fact, the transmission loss $L\,oss_t$ from experiment mainly arises from the coupling loss $L\,oss_c$ [27], the intrinsic loss $L\,oss_i$ [28] and the scattering loss $L\,oss_\sigma$ induced by roughness [19]–[22]. For the SMFW and MMFW structures, $L\,oss_c^{(s)} \approx L\,oss_c^{(m)}$ and $L\,oss_i^{(s)} \approx L\,oss_i^{(m)}$. The relationship between

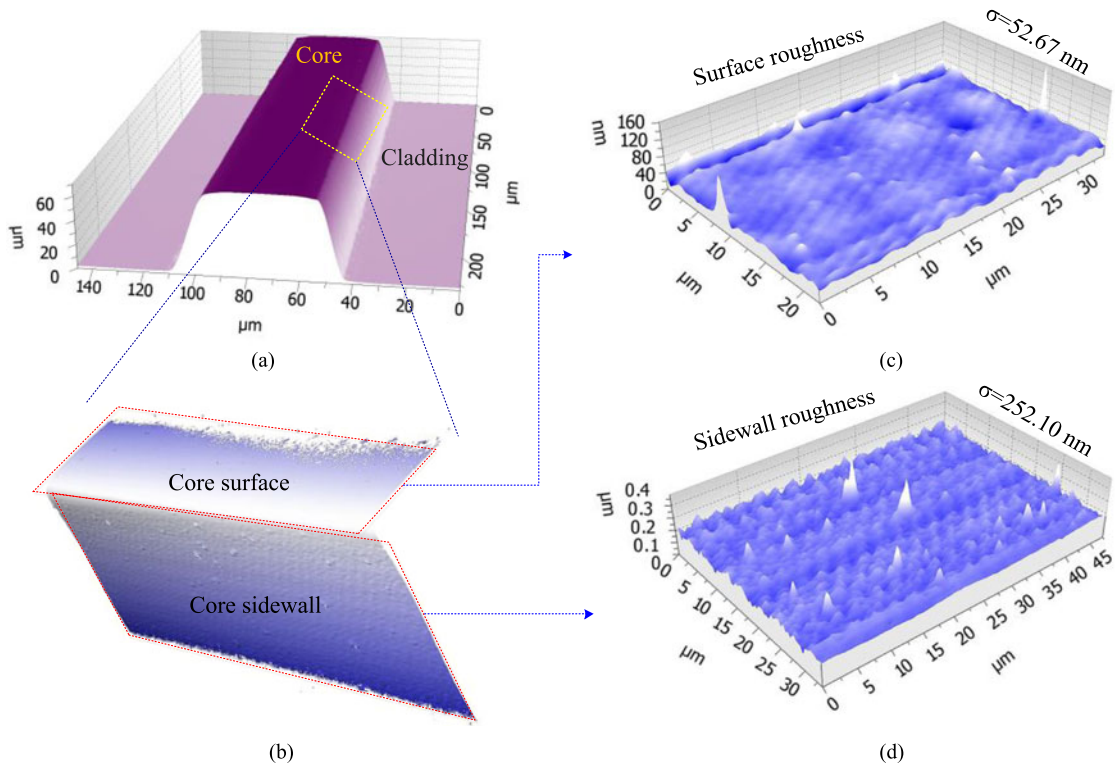

Fig. 9. Measurement results of ROW. (a) Microscopic appearance of ROW, (b) enlarged details of core surface and core sidewall, (c) core surface roughness, and (d) core sidewall roughness.

TABLE 2
Random Values Along Core

Num.	σ/nm	Num.	σ/nm	Num.	σ/nm
1	309.07	5	268.04	9	274.75
2	288.31	6	285.67	10	272.64
3	282.72	7	253.05	11	252.10
4	283.116	8	292.24	12	242.75

$L\,oss_t^{(s)}$ and $L\,oss_t^{(m)}$ can be expressed as

$$\delta = L\,oss_t^{(m)} - L\,oss_t^{(s)} = \left(L\,oss_c^{(m)} + L\,oss_i^{(m)} + L\,oss_\sigma^{(m)}\right) - \left(L\,oss_c^{(s)} + L\,oss_i^{(s)} + L\,oss_\sigma^{(s)}\right)$$
$$\approx L\,oss_\sigma^{(m)} - L\,oss_\sigma^{(s)}. \quad (8)$$

In our experiment, the field radius of LD laser is constant at the micron scale. In order to obtain the efficient coupling between the light source and MMF (50/125 μm, Corning Inc.), thin-core-fiber-MMF structure is adopted. A piece of thin-core fiber with $\omega_l = 2.5\,\mu$m can be considered as the driving source to MMF. The ROW endface is polished by the sandpaper and the endface roughness is estimated to be 7.67 nm as shown in Fig. 10(a). Based on the scalar scattering theory [28], the

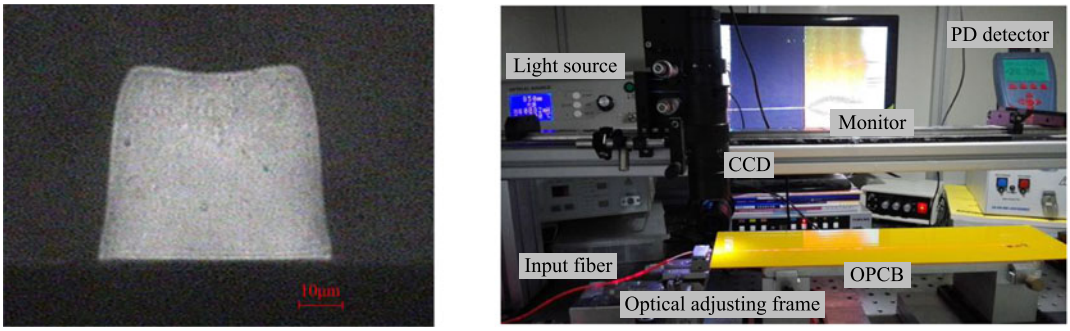

(a) (b)

Fig. 10. Experimental measurement of transmission loss. (a) ROW core endface polished and (b) physical map of the experiment device.

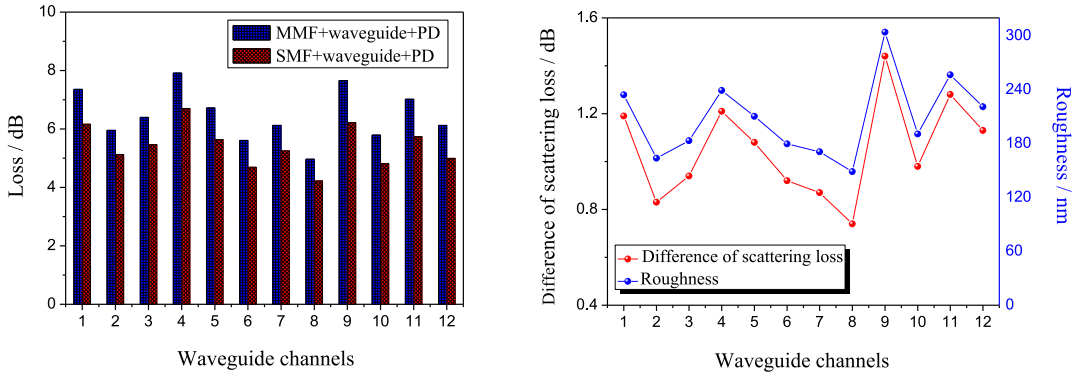

(a) (b)

Fig. 11. Experimental measurement results. (a) Transmission loss test of ROW for SMFW and MMFW, and (b) difference of transmission loss for SMFW and MMFW structures and roughness calculated.

TABLE 3
Twelve Groups of Data About σ as δ

Channels	δ/dB	σ/nm	Channels	δ/dB	σ/nm	Channels	δ/dB	σ/nm
1	1.19	234.37	5	1.08	210.37	9	1.44	304.08
2	0.83	163.83	6	0.92	179.65	10	0.98	190.71
3	0.94	183.28	7	0.87	170.77	11	1.28	256.50
4	1.21	239.07	8	0.74	148.70	12	1.13	220.93

endface scattering loss only is 0.05 dB, which can be neglected. In order to decrease the coupling loss further, index matching liquid has been applied on the connection between fiber and ROW. The input fiber is adjusted by a 6-D stage to be aimed at the ROW core.

We further measure the transmission loss of OPCBs (from TTM Technologies, Inc) with the length of 41.5 cm. Fig. 10(b) shows the experimental setup. The transmission losses of ROW for the SMFW structure and for the MMFW structure are shown in Fig. 11(a). It can be seen that the transmission loss for the MMFW structure is larger than that for the SMFW structure. The difference δ is in range

of 0.8-1.5 dB, which is shown as Fig. 11(b). It indicates the correctness of the coupled-mode theory used to explaining the scattering loss of ROW. Table 3 gives 12 groups of σ with corresponding δ, for example, σ is 163.83 nm when δ is 0.83 dB.

5. Conclusion

In this work, we reported a simple method to estimate the roughness of multimode ROW based on the differential scattering loss induced by roughness between for the SMFW structure and for the MMFW structure. By using the coupled-mode theory, the coupling characteristics between fiber (SMF and MMF) and ROW for the two kinds of coupled structures is analyzed in detail. The mode scattering loss coefficient of ROW induced by the roughness is simulated, and further the total scattering loss coefficient is obtained. The results indicate that the scattering loss for the MMFW structure is larger than that for the SMFW structure. Based on the scattering loss difference between for the SMFW structure and for the MMFW structure, a method to estimate the roughness of ROW is proposed. The simulated data shows that the difference of scattering loss increases with increasing roughness. The experimental results show that the roughness is 248.67 nm when the waveguide length is 75 mm and the scattering loss difference is 0.31 dB, and the roughness by 3-D optical profiler is 275.37 nm, which well conforms to the experimental measurement results based on the proposed method. Thus, it is proved that the proposed method for roughness estimation is effective.

Appendix A

According to the [17], $K^{i}_{mn,\rho}(\kappa, \upsilon)$ can be expressed as [25]

$$K^{1}_{mn,\rho}(\kappa, \upsilon) = \frac{\omega\varepsilon_0}{4iP} a^{*}_{mn} a_\rho \delta n \left(\frac{n_1}{n_2}\right)^2 \sin(k_x\xi) f_1(z) \cdot Q(k_y, \eta, \kappa) \tag{A.1}$$

$$K^{2}_{mn,\rho}(\kappa, \upsilon) = -\frac{\omega\varepsilon_0}{4iP} a^{*}_{mn} a_\rho \delta n \cos(k_y\eta) f_2(z) \cdot P(k_x, \xi, \upsilon) \tag{A.2}$$

where $K^{1}_{mn,\rho}(\kappa, \upsilon)$ and $K^{2}_{mn,\rho}(\kappa, \upsilon)$ is related to the core surface ① and the core sidewall ②, respectively. For E^{x}_{mn} mode, k_x and k_y are the transversal propagation constant to x and y direction, η and ξ are phase parameters, and a_{mn} is the normalization factor of the electrical field. For the radiation mode, κ and υ are the propagation vector in x and y directions, and a_ρ is the normalization factor of the electrical field. $Q(k_y, \eta, \kappa)$ and $P(k_x, \xi, \upsilon)$ can be written as [24]

$$Q(k_y, \eta, \kappa) = \int_0^b \exp(i\kappa y)\cos\left[k_y(y+\eta)\right] dy \tag{A.3}$$

$$P(k_x, \xi, \upsilon) = \int_0^{-a} \exp(i\upsilon x)\sin\left[k_x(x+\xi)\right] dx. \tag{A.4}$$

$F^{i}(\beta_{mn} - \beta_\rho)$ is the Fourier transform of the roughness function $f(z)$ calculated at the difference between the guided modes and the radiation modes, which can be written as [17]

$$\left|F^{1}(\beta_{mn} - \beta_\rho)\right|^2 = \sigma_1^2\sqrt{\pi}L_c \cdot \exp\left[-\left(\frac{(\beta_{mn} - \beta_\rho)L_c}{2}\right)^2\right] \tag{A.5}$$

$$\left|F^{2}(\beta_{mn} - \beta_\rho)\right|^2 = \sigma_2^2\sqrt{\pi}L_c \cdot \exp\left[-\left(\frac{(\beta_{mn} - \beta_\rho)L_c}{2}\right)^2\right] \tag{A.6}$$

where $F^{1}(\beta_{mn} - \beta_\rho)$ and $F^{2}(\beta_{mn} - \beta_\rho)$ is related to the roughness σ_1 at the core surface ① and the roughness σ_2 at the core sidewall ② β_{mn} and β_ρ is the propagation constant of the guided modes

and the radiation modes in z direction, respectively, which can be expressed as [25]

$$\beta_{mn} = \sqrt{(n_1 k)^2 - {k_x}^2 - {k_y}^2} \tag{A.7}$$

$$\beta_{\rho} = \sqrt{(n_2 k)^2 - \kappa^2 - \upsilon^2}. \tag{A.8}$$

The expressions for $(K^3_{mn,\rho}(\kappa, \upsilon), |F^3(\beta_{mn} - \beta_{\rho})|^2)$ and $(K^4_{mn,\rho}(\kappa, \upsilon), |F^4(\beta_{mn} - \beta_{\rho})|^2)$ are analogous and are therefore omitted here.

Appendix B

For the SMFW structure, when SMF is coupled to ROW, the coupling efficiency between $L\,P_{01}$ mode of SMF and E^x_{mn} mode of ROW can be expressed as

$$\eta_{s\to mn} = \frac{\left|\int_{-\infty}^{\infty}\int_{-\infty}^{\infty} \psi_s(x,y)\,\psi_{mn}(x,y)\,dxdy\right|^2}{\int_{-\infty}^{\infty}\int_{-\infty}^{\infty} |\psi_s(x,y)|^2 dxdy \int_{-\infty}^{\infty}\int_{-\infty}^{\infty} |\psi_{mn}(x,y)|^2 dxdy} \tag{B.1}$$

where $\psi_s(x, y)$ is $L\,P_{01}$ mode field distribution of SMF, and $\psi_{mn}(x, y)$ is E^x_{mn} mode field distribution. Considering all the supported modes in ROW, the total coupling efficiency between SMF and ROW can be expressed as

$$\eta_{s\to w} = \sum_{m=1}^{M}\sum_{n=1}^{N} |\eta_{s\to mn}| \tag{B.2}$$

where M and N is the total mode order of ROW for m and n, respectively.

Within the MMFW structure, a number of $L\,P_{0q}$ modes of MMF can be found under the weakly guiding approximation, where q is the mode order. The mode coupling efficiency between $L\,P_{0q}$ mode and E^x_{mn} mode can be written as

$$\eta_{q\to mn} = \frac{\left|\int_{-\infty}^{\infty}\int_{-\infty}^{\infty} \psi_q(x,y)\,\psi_{mn}(x,y)\,dxdy\right|^2}{\int_{-\infty}^{\infty}\int_{-\infty}^{\infty} |\psi_q(x,y)|^2 dxdy \int_{-\infty}^{\infty}\int_{-\infty}^{\infty} |\psi_{mn}(x,y)|^2 dxdy} \tag{B.3}$$

where $\psi_q(x, y)$ is LP_{0q} mode field distribution of MMF. Considering all the supported modes in MMF and in ROW, the total coupling efficiency between MMF and ROW can be written as

$$\eta_{m\to w} = \sum_{q=1}^{Q} |\eta_{l\to q}| \left[\sum_{m=1}^{M}\sum_{n=1}^{N} |\eta_{q\to mn}|\right] \tag{B.4}$$

where Q is the total mode order of MMF, $\eta_{l\to q}$ is the coupling efficiency between light source and $L\,P_{0q}$ modes of MMF.

Acknowledgment

The authors would like to thank the optical interconnection research team for their valuable suggestions from TTM Technologies, Inc.

References

[1] M. A. Taubenblatt, "Optical interconnects for high-performance computing," *J. Lightw. Technol.*, vol. 30, no. 4, pp. 448–457, Feb. 2012.
[2] C. Kachris and I. Tomkos, "A survey on optical interconnects for data centers," *IEEE Commun. Surveys Tut.*, vol. 14, no. 4, pp. 1021–1036, Jan. 2012.
[3] J. Matsui *et al.*, "Optical interconnect architecture for servers using high bandwidth optical mid-plane," in *Proc. Opt. Fiber Commun. Conf. Expo.*, 2012, Paper OW3J.6.
[4] A. Ghiasi, "Large data centers interconnect bottlenecks," *Opt. Exp.*, vol. 23, no. 3, pp. 2085–2090, Feb. 2015.

[5] R. Dangel *et al.*, "Development of versatile polymer waveguide flex technology for use in optical Interconnects," *J. Lightw. Technol.*, vol. 31, no. 24, pp. 3915–3926, Dec. 2013.
[6] L. Brusberg, S. Whalley, C. Herbst, and H. Schröder, "Display glass for low-loss and high-density optical interconnects in electro-optical circuit boards with eight optical layers," *Opt. Exp.*, vol. 23, no. 25, pp. 32528–32540, Dec. 2015.
[7] M. Heinrich *et al.*, "Supersymmetric mode converters," *Nature Commun.*, vol. 5, Apr. 2014, Art. no. 3698.
[8] N. Hendrickx *et al.*, "Embedded micromirror inserts for optical printed circuit boards," *IEEE Photon. Technol. Lett.*, vol. 20, no. 20, pp. 1727–1729, Oct. 2008.
[9] J. Chen *et al.*, "High bandwidth and large coupling tolerance graded-index multimode polymer waveguides for on-board high-speed optical interconnects," *J. Lightw. Technol.*, vol. 34, no. 12, pp. 2934–2940, Jun. 2016.
[10] N. Bamiedakis *et al.*, "40 Gb/s data transmission over a 1 m long multimode polymer spiral waveguide for board-level optical interconnects," *J. Lightw. Technol.*, vol. 33, no. 4, pp. 882–888, Feb. 2015.
[11] R. Sun *et al.*, "Impedance matching vertical optical waveguide couplers for dense high index contrast circuits," *Opt. Exp.*, vol. 16, no. 16, pp. 11682–11690, Aug. 2008.
[12] M. Liu *et al.*, "A graphene-based broadband optical modulator," *Nature*, vol. 474, pp. 64–67, May 2011.
[13] J. A. Frantz, L. B. Shaw, J. S. Sanghera, and I. D. Aggarwal, "Waveguide amplifiers in sputtered films of Er3+-doped gallium lanthanum sulfide glass," *Opt. Exp.*, vol. 14, no. 5, pp. 1797–1803, Mar. 2006.
[14] C. Y. Chao, W. Fung, and L. J. Guo, "Polymer microring resonators for biochemical sensing applications," *IEEE J. Sel. Topics Quantum Electron.*, vol. 12, no. 1, pp. 134–142, Jan. 2006.
[15] J. L. Dong, K. S. Chiang, and W. Jin, "Compact three-dimensional polymer waveguide mode multiplexer," *J. Lightw. Technol.*, vol. 33, no. 22, pp. 4580–4588, Nov. 2015.
[16] A. Neyer, S. Kopetz, E. Rabe, W. J. Kang, and S. Tombrink, "Electrical-optical circuit board using polysiloxane optical waveguide layer," in *Proc. 55th Electron. Compon. Technol. Conf.*, 2005, pp. 246–250.
[17] D. Donato *et al.*, "Stationary mode distribution and sidewall roughness effects in overmoded optical waveguides," *J. Lightw. Technol.*, vol. 28, no. 10, pp. 1510–1520, May 2010.
[18] K. Halbe and E. Griese, "A modal approach to mode integrated optical waveguides with rough core-cladding-interfaces," in *Proc. IEEE Workshop Signal Propag. Interconnects*, 2006, pp. 133–136.
[19] F. P. Payne and J. P. R. Lacey, "A theoretical analysis of scattering loss from planar optical waveguides," *Opt. Quantum Electron.*, vol. 26, no. 10, pp. 977–986, Oct. 1994.
[20] K. K. Lee, D. R. Lim, H.-C. Luan, A. Agarwal, J. Foresi, and L. C. Kimerling, "Effect of size and roughness on light transmission in a Si/SiO2 waveguide: Experiments and mode," *Appl. Phys. Lett.*, vol. 77, no. 11, pp. 1616–1619, Jul. 2000.
[21] F. Grillot, L. Vivien, S. Laval, and E. Cassan, "Propagation loss in single-mode ultrasmall square silicon-on-insulator optical waveguides," *J. Lightw. Technol.*, vol. 24, no. 2, pp. 891–896, Feb. 2006.
[22] E. Jaberansary *et al.*, "Scattering loss estimation using 2-D fourier analysis and modeing of sidewall roughness on optical waveguides," *IEEE Photon J.*, vol. 5, no. 3, Jun. 2013, Art. no. 6601010.
[23] S. Khademzadeh, S. Carmignato, N. Parvin, F. Zanini, and P. F. Bariani, "Micro porosity analysis in additive manufactured NiTi parts using micro computed tomography and electron microscopy," *Mater. Design*, vol. 90, pp. 745–752, Nov. 2016.
[24] E. A. J. Marcatili, "Dielectric rectangular waveguide and directional coupler for integrated optics," *Bell Syst. Tech. J.*, vol. 48, pp. 2071–2102, Sep. 1969.
[25] D. Lenz, D. Erni, and W. Bachtold, "Modal power loss coefficients for highly overmoded rectangular dielectric waveguides based on free space modes," *Opt. Exp.*, vol. 12, no. 6, pp. 1150–1156, Mar. 2004.
[26] E. Griese, "Modeling of highly multimode waveguides for time-domain simulation," *IEEE J. Sel. Topics Quantum Electron.*, vol. 9, no. 2, pp. 433–442, Mar. 2003.
[27] H. L. Hsiao *et al.*, "Compact and passive-alignment 4–channel × 2.5 Gbps optical interconnect modules based on silicon optical benches with 45° micro-reflectors," *Opt. Exp.*, vol. 17, no. 26, pp. 24250–24260, Dec. 2009.
[28] K. Peters, "Polymer optical fiber sensors-a review," *Smart Mater. Struct.*, vol. 20, pp. 1–17, Dec. 2011.
[29] Y. J. Wang, Z. L. Lin, X. L. Cheng, C. S. Zhang, F. Gao, and F. Zhang, "Scattering loss in silicon-on-insulator rib waveguides fabricated by inductively coupled plasma reactive ion etching," *Appl. Phys. Lett.*, vol. 85, no. 18, pp. 3995–3997, Nov. 2004.